Electronic Supplementary Material (ESI) for Analytical Methods.
This journal is © The Royal Society of Chemistry 2021

Supporting information for

Sensitive Fluorescence and Visual Detection of Organophosphorus Pesticides with $Ru(bpy)_3^{2+}$-ZIF-90-MnO_2 Sensing Platform

Jun Li[a, †], Yingwei Weng[a, †], Can Shen[a], Jiao Luo[a], Donghong Yu[b], Zhong Cao[a,*]

[a]Hunan Provincial Key Laboratory of Materials Protection for Electric Power and Transportation, and Hunan Provincial Key Laboratory of Cytochemistry, School of Chemistry and Biological Engineering, Changsha University of Science and Technology, Changsha, 410114, P. R. China

[b]Department of Chemistry and Bioscience, Aalborg University, DK-9220 Aalborg, East, Denmark

[†]J. L. and Y. W. as the co-first authors contributed equally to this work.

*To whom correspondence should be addressed. *E*-mail: caoz@csust.edu.cn

Chemicals and Instruments

Zinc acetate ($Zn(CH_3COO)_2$) and Imidazolate-2-carboxyaldehyde (2-ICA) were purchased from Titan Scientific Co., Ltd. (Shanghai, China) and Macklin Biochemical Co., Ltd. (Shanghai, China). Tetramethylammonium hydroxide, glycine (Gly), L-glutamic acid (L-Glu), and manganese chloride ($MnCl_2 \cdot 4H_2O$) were supplied by Sinopharm Chemical Reagent Co., Ltd.. Acetylcholinesterase (AChE, 500 units, from Electrophorus electricus), bovine serum albumin (BSA), catalase (CAT), L-cysteine (L-Cys), and glucose oxidase (GOx) were bought from Sigma-Aldrich Co., Ltd.. Acetylthiocholine (ATCh) iodide, parathion-methyl, dichlorvos, chlorpyrifos, paraquat, fenvalerate, tris-(2-terephthalic acid 2'-bipyridine), imidacloprid, acetochlor, nitenpyram, and ruthenium dichloride ($Ru(bpy)_3Cl_2 \cdot 6H_2O$, >98%) were supplied by Aladdin Biochemical Technology Co., Ltd. (Shanghai, China). Malathion, omethoate and paraoxon were offered by Huaerbo Technology Co., Ltd. (Beijing, China). Milli-Q water (18.2 $M\Omega \cdot cm^{-1}$) was employed for experimental sample preparation.

Scanning electron microscopic (SEM, SU8010, Hitachi), transmission electron microscopy (TEM, Talos F200X), and high-annular dark-field scanning TEM (HAADF-STEM) images with an energy dispersed X-ray detector (EDX) were used for detailed composition analysis of the prepared samples. Powder X-ray diffraction (PXRD) measurements were carried out on a D8-ADVANCE powder diffractometer. Nitrogen adsorption-desorption isotherm was obtained on a Micromeritics ASAP 2460 Sorptometer. The surface potential was measured using a nanoparticle size and zeta potentiometer (Zetasizer Nano ZS90, Malvern Instruments, UK). The UV-2700 spectrophotometer (Shimadzu Co., Japan) was used to collect the UV-Vis spectra. The fluorescent emission spectra were recorded by the F-7000 fluorescence spectrophotometer (Hitachi Co., Japan).

Synthesis of ZIF-90

ZIF-90 was synthesized using the reported method.[1] $Zn(CH_3COO)_2$ (73.3 mg, 0.1 M) and imidazolate-2-carboxyaldehyde (2-ICA) (76.9 mg, 0.2 M) were separately dissolved in 4 mL DMF solution. Under vigorous stirring, the as-prepared two solution were mixed. After 5 min, another 10 mL of DMF was added into the mixture to further stabilize the crystal products about 30 min, and then centrifugation and washing with DMF and ethanol for three times. Finally, the resulting solid was dried overnight at 60 °C under vacuum for further use.

Construction of $Ru(bpy)_3^{2+}$-ZIF-90-MnO_2

10 μL of the synthesized $Ru(bpy)_3^{2+}$-ZIF-90 (1 mg/mL) and 225 μL of the prepared MnO_2 NSs solution were mixed in 265 μL of PBS (10 mM, pH 7.0). And then the resulted aqueous suspension was further incubated for 10 min to form the $Ru(bpy)_3^{2+}$-ZIF-90-MnO_2 composites.

Detection Procedure for AChE

Various concentrations of AChE (50 μL) were incubated with ATCh (25 mM, 100 μL) for 20 min at 37 °C. Then, MnO_2 NSs (2 mg/mL, 225 μL) and $Ru(bpy)_3^{2+}$-ZIF-90 (1 mg/mL, 10 μL) were added to the above solution. Subsequently, the mixture was diluted to 500 μL with PBS (10 mM, pH 7.0) and mixed thoroughly for 10 min before the fluorescence spectra were collected at an excitation wavelength of 450 nm.

OPs Detection in Real Samples

This proposed strategy was employed to detect parathion-methyl in environmental and agricultural samples, including lake water, tap water and cabbage samples. The lake water (10 mL) was filtered with a 0.22 μm filter membrane to remove insoluble materials and the tap water (10 mL) was boiled to remove chlorine. Then, the processed water samples mixed with 10 mL PBS (10 mM, pH 7.4) containing 20 % methanol. The cabbage (10 g) was ground and mixed with 50 mL of acetonitrile under sonication for 10 min and centrifuged to get the supernatant. This extraction procedure was repeated for three times, and the extract was combined and evaporated to dryness, followed by dissolved by PBS (10 mM, pH 7.4) containing 20 % methanol. Subsequently, the prepared three samples were spiked with 5, 20 and 50 ng/mL parathion-methyl standards, respectively. The recovery rates (%) and relative standard deviations (RSD) (n=3, %) were calculated to evaluate the value of the strategy.

Data

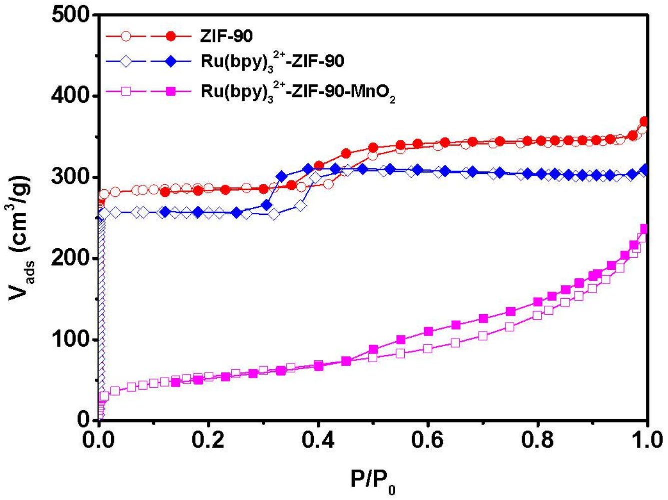

Fig. S1. N_2 sorption isotherms of ZIF-90, $Ru(bpy)_3^{2+}$-ZIF-90, and $Ru(bpy)_3^{2+}$-ZIF-90-MnO_2 composites. The BET surface areas of the three samples are 1064, 951, and 192 m^2/g, respectively. (Filled and open symbols represent desorption and adsorption branches, respectively).

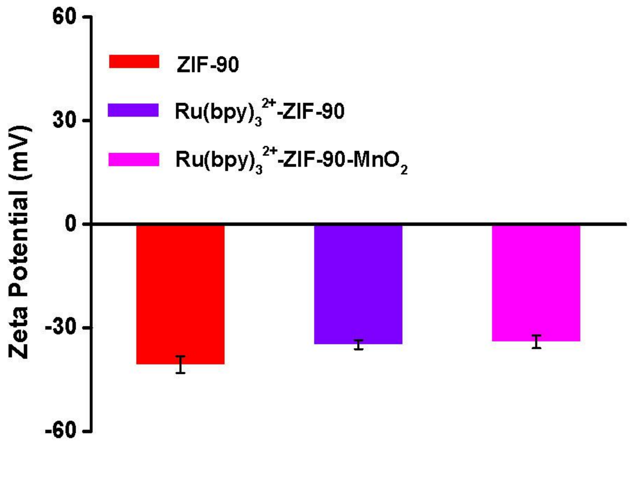

Fig. S2. Zeta potentials of ZIF-90, $Ru(bpy)_3^{2+}$-ZIF-90, and $Ru(bpy)_3^{2+}$-ZIF-90-MnO_2. Error bars indicate s.d. (n = 3).

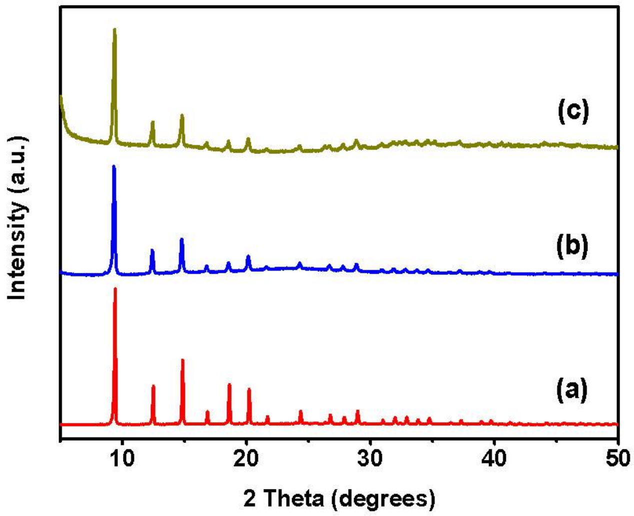

Fig. S3. Powder X-ray diffraction (XRD) profiles of (a) as-synthesized ZIF-90, (b) $Ru(bpy)_3^{2+}$-ZIF-90, and (c) $Ru(bpy)_3^{2+}$-ZIF-90 immersed in water for 24 h.

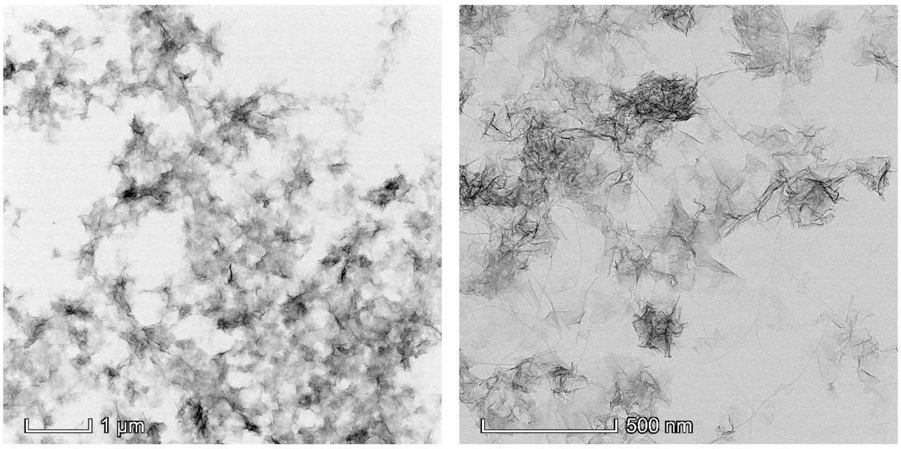

Fig. S4. TEM images of MnO_2 at different magnifications.

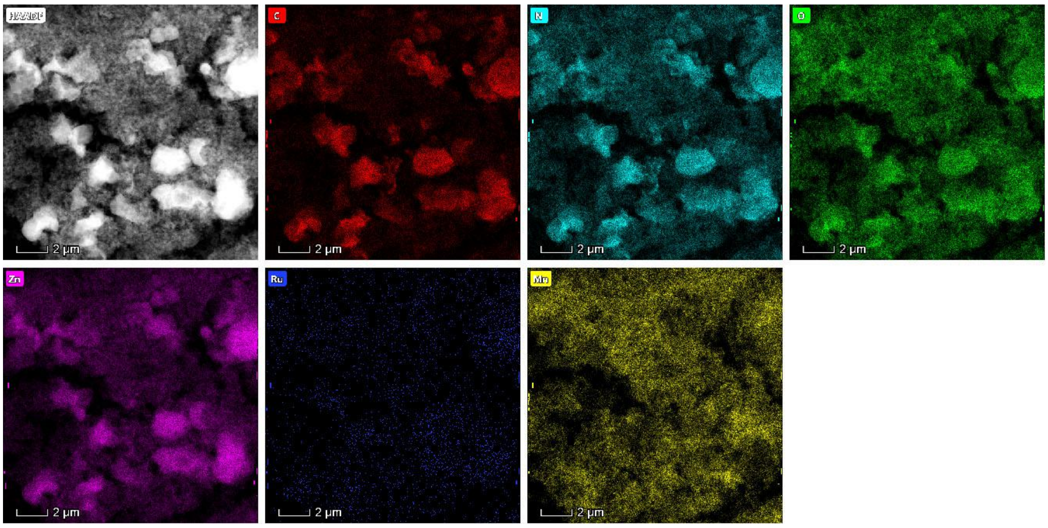

Fig. S5. HAADF-STEM image and elemental mappings of $Ru(bpy)_3^{2+}$-ZIF-90-MnO_2 under high resolution revealing the elemental distribution.

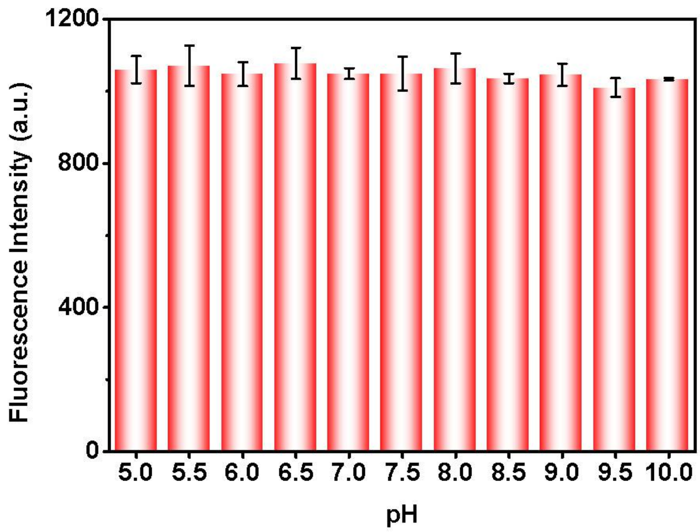

Fig. S6. Fluorescence intensity of the $Ru(bpy)_3^{2+}$-ZIF-90 fluorescent probe at different pH values. Error bars indicate s.d. (n = 3).

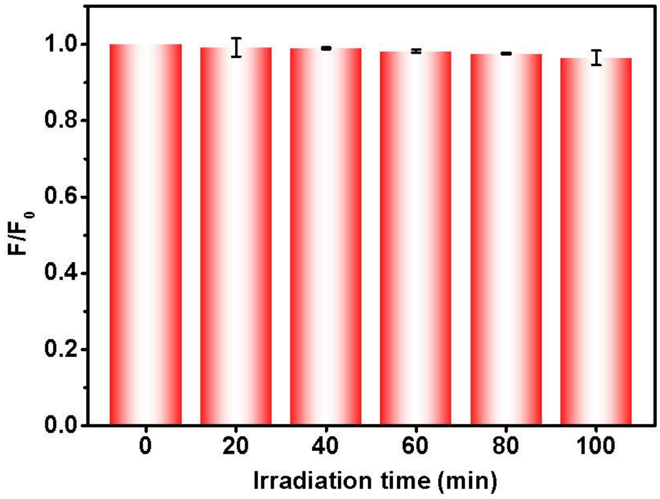

Fig. S7. Stability of photoluminescence of the $Ru(bpy)_3^{2+}$-ZIF-90 fluorescent probe under the UV lamp. Where F_0 and F are the fluorescence intensity of $Ru(bpy)_3^{2+}$-ZIF-90 fluorescent probe under UV light for 0 min and different times, respectively. Error bars indicate s.d. (n = 3).

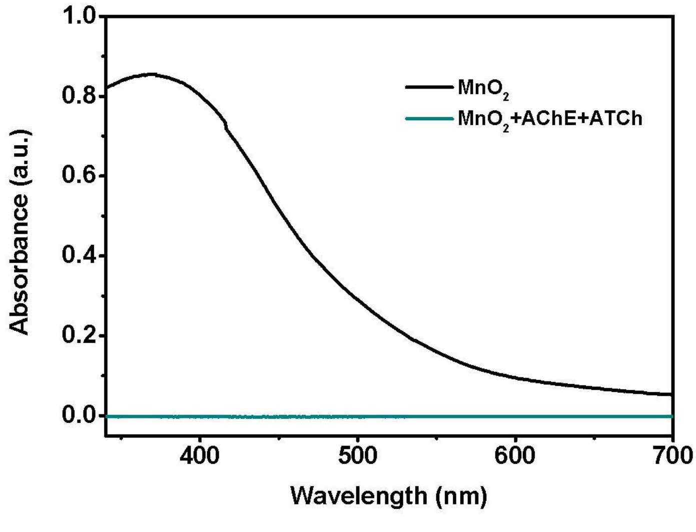

Fig. S8. The UV-vis absorption spectra of MnO_2 NSs in the absence and presence of AChE+ATCh.

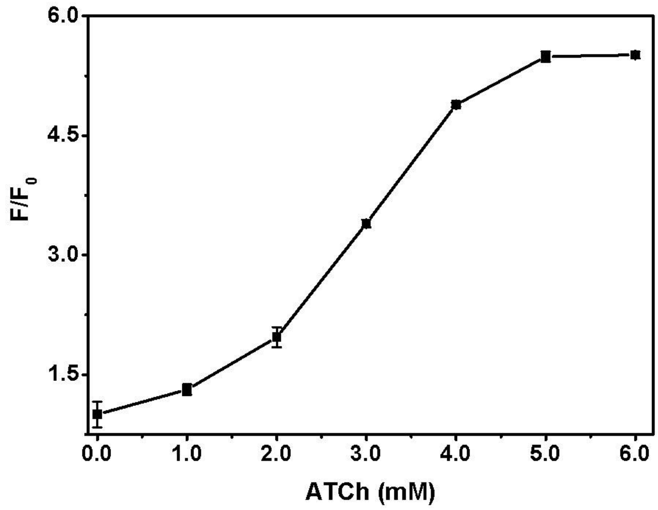

Fig. S9. The relative fluorescence enhancement (*F*/*F_0*) under different concentrations of ATCh (0, 1.0, 2.0, 3.0, 4.0, 5.0, and 6.0 mM final solution). The fluorescence signal was collected at 600 nm. Where *F* and *F_0* are the fluorescence intensity of the $Ru(bpy)_3^{2+}$-ZIF-90-MnO_2-AChE mixture in the presence and absence of ATCh, respectively. Error bars indicate s.d. (n = 3).

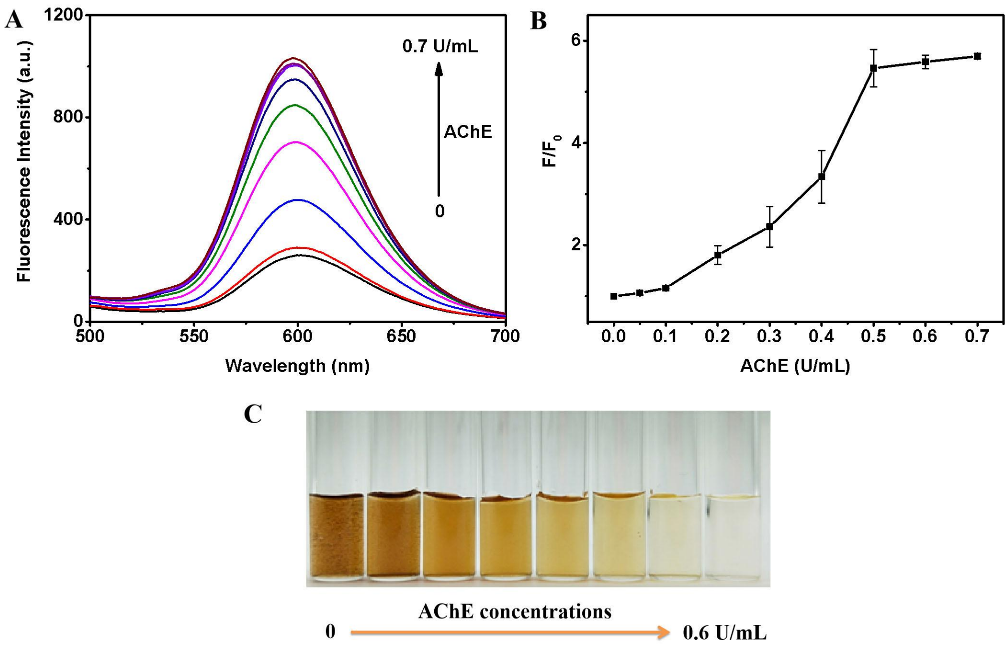

Fig. S10. (A) The fluorescence spectra of $Ru(bpy)_3^{2+}$-ZIF-90-MnO_2-ATCh mixture with various concentrations of AChE. Final concentrations of AChE are 0, 0.05, 0.1, 0.2, 0.3, 0.4, 0.5, 0.6, and 0.7 U/mL. (B) The F/F_0 under different concentrations of ATCh. Where F and F_0 are the fluorescence intensity of the $Ru(bpy)_3^{2+}$-ZIF-90-MnO_2-ATCh mixture in the presence and absence of AChE. (C) The corresponding photographs of the system taken under sunlight.

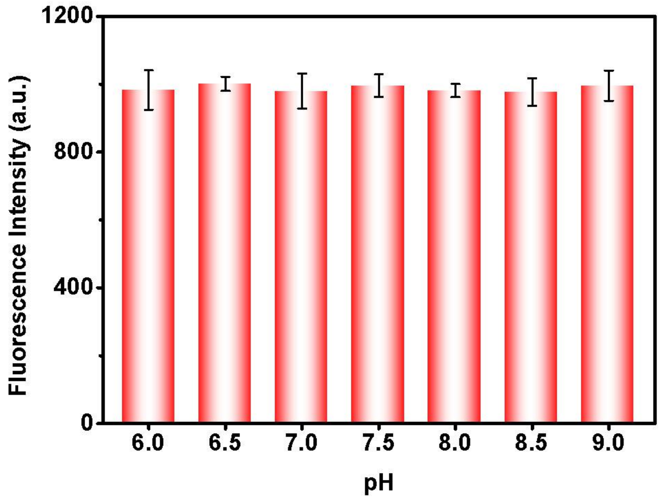

Fig. S11. Fluorescence intensity of the $Ru(bpy)_3^{2+}$-ZIF-90-MnO_2+AChE-ATCh sensing system under different pH conditions. Error bars indicate s.d. (n = 3).

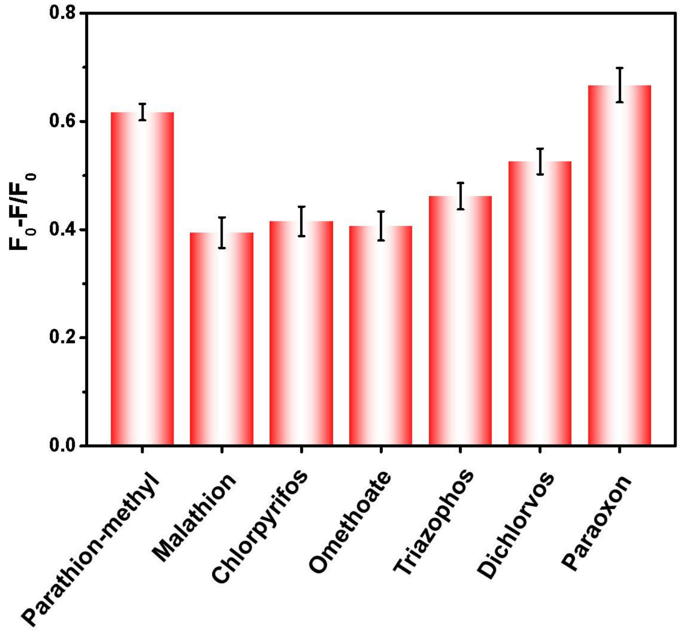

Fig. S12. Other OPs determination based on the inhibition efficiency ((F_0-F)/F_0) of AChE. F and F_0 were the fluorescence intensity of the sensing system in the presence and absence of the different OPs. The concentrations of parathion-methyl, malathion, chlorpyrifos, omethoate, triazophos, dichlorvos, and paraoxon were all 20 ng/mL.

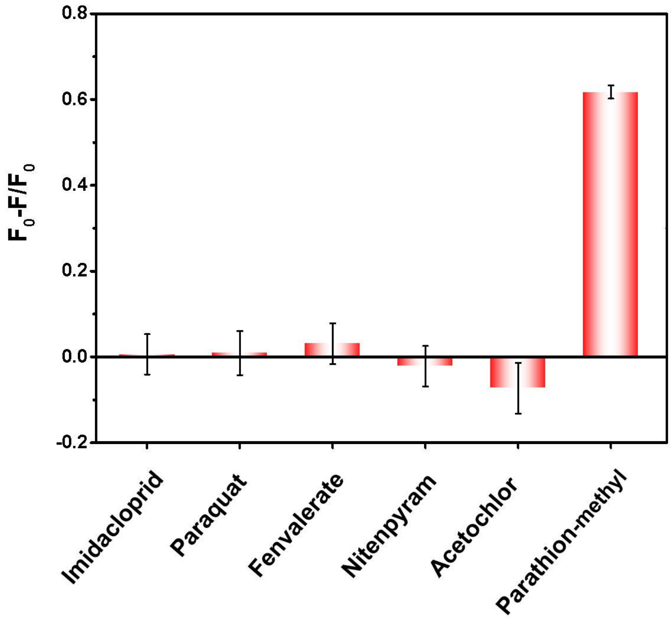

Fig. S13. The other kind of pesticides determination based on the inhibition efficiency ((F_0-F)/F_0) of AChE. F and F_0 were the fluorescence intensity of the sensing system in the presence and absence of the different pesticides. The concentrations of imidacloprid, paraquat, fenvalerate, nitenpyram, acetochlor, and parathion-methyl were all 20 ng/mL.

Table S1 Comparison of performance of different parathion-methyl probing strategy

Method	Linear range (ng/mL)	Detection limit (ng/mL)	Reference
Electrochemical assay	$132\text{-}3.9\times10^4$	5.3	[2]
Electrochemical assay	$0.40\text{-}7.0\times10^3$	0.10	[3]
Electrochemistry assay	$0.26\text{-}4.6\times10^4$	0.045	[4]
Electrochemistry assay	0.080-5.3 5.3-40	0.024	[5]
Enzyme-linked immunosorbent assay	0.40-19	0.20	[6]
Fluorescence assay	$1.0\text{-}1.0\times10^3$	0.12	[7]
Fluorescence assay	$70\text{-}5.0\times10^3$	0.12	[8]
Fluorescence assay	$197\text{-}5.3\times10^3$	25	[9]
Chemiluminescence enzyme assay	$0.50\text{-}1.0\times10^3$	0.50	[10]
Fluorescence and visual assay	0.050-60	0.037	This work

Table S2 Detection of parathion-methyl in environmental and agricultural samples

Sample	Spiked (ng/mL)	Detected (ng/mL)	Recovery (%)	RSD (n=3, %)
Lake water	5	4.81	96.2	6.2
	20	18.70	93.5	5.2
	50	49.14	98.3	5.6
Tap water	5	4.98	99.5	2.3
	20	20.73	103.6	6.7
	50	48.52	97.0	5.9
Cabbage	5	4.67	93.3	4.1
	20	18.95	94.7	2.1
	50	48.63	97.3	2.5

References

[1] J. J. Deng, K. Wang, M. Wang, P. Yu and L. Q. Mao, *J. Am. Chem. Soc.*, 2017, **139**, 5877-5882.

[2] X. Y. Gao, Y. Gao, C. C. Bian, H. Y. Ma and H. L. Liu, *Electrochim. Acta.*, 2019, **310**, 78-85.

[3] T. Tao, Y. Zhou, C. H. He, H. P. He, M. Y. Ma, Z. W. Cai, N. Gao, K. Wang, R. Z. Zhu, G. Chang, Z. H. Liu and Y. B. He, *Electrochim. Acta.*, 2020, **357**, 136836.

[4] K. P. Gannavarapu, V. Ganesh, M. Thakkar, S. Mitra and R. B. Dandamudi, *Sens Actuators B Chem.*, 2019, **288**, 611-617.

[5] J. Y. Yao, Z. P. Liu, M. L. Jin, Y. Y. Zou, J. M. Chen, P. Xie, X. Wang, E. M. Akinoglu, G. F. Zhou and L. L. Shui, *Sens. Actuators B Chem.*, 2020, **321**, 128517.

[6] L. P. Yuan, B. Liu, K. D. Yin, G. D. Yang, L. Huang and Y. H. Nie, *Anal. Lett.*, 2013, **46**, 1084-1096.

[7] X. H. Xu, Y. N. Guo, X. Y. Wang, W. Li, P. P. Qi, Z. W. Wang, X. Q. Wang, S. Gunasekaran and Q. Wang, *Sens. Actuators B Chem.*, 2018, **260**, 339-345.

[8] K. Y. He, Z. S. Li, L. Wang, Y. C. Fu, H. R. Quan, Y. B. Li, X. Q. Wang, S.

Gunasekaran and X. H. Xu, *ACS Appl. Mater. Interfaces*, 2019, **11**, 26250-26260.

[9] X. Hu, F. Y. Wang, Q. Q. Peng, J. Hu, H. Q. Peng, L. Li, B. Z. Zheng, J. Du and D. Xiao, *RSC Adv.*, 2019, **9**, 13048-13053.

[10] R. K. Mishra, K. Deshpande and S. Bhand, *Sensors*, 2010, **10**, 11274-11286.